forests

MDPI

Article

Integrated Transcriptome and Metabolome Analysis Reveals Molecular Mechanisms of Flavonoid Biosynthesis During *Camphora officinarum* Leaf Development

Xiaofeng Peng [1], Peiwu Xie [2], Bing Li [2], Yonglin Zhong [2], Boxiang He [2], Yingli Wang [2], Yiqun Chen [2], Ning Li [1] and Chen Hou [2,*]

[1] College of Forestry, Central South University of Forestry and Technology, Changsha 410004, China; nli@csuft.edu.cn (N.L.)
[2] Guangdong Provincial Key Laboratory of Silviculture, Protection and Utilization, Guangdong Academy of Forestry, Guangzhou 510520, China
* Correspondence: houchen@sinogaf.cn

Abstract

Camphora officinarum Nees is a significant economic tree because of its aromatic, medicinal, and ornamental attributes. The diverse flavonoids present within the leaves of *C. officinarum* have been neglected for an extended period, hindering a comprehensive understanding of the molecular mechanisms responsible for color transformation and resistance to adverse environmental conditions. In this study, multi-omics analyses were conducted to systematically compare the relative contents of flavonoid metabolites and the expression profiles of flavonoid-related genes across three developmental stages of *C. officinarum* leaves. A total of 175 flavonoid compounds were detected via metabolomics, with flavonols being the most abundant. Through weighted gene co-expression network analysis, 25 key DEGs encoding *CHS*, *DFR*, *FLS*, *ANS*, *F3′H,* and *LAR* genes are predicted to be involved in anthocyanin biosynthesis for color change during leaf development. Notably, ten MYB, seven bHLH, and three ERF factors are potentially implicated in the regulation of key genes, underscoring their significant contributions to the color mechanisms underlying flavonoid biosynthesis. Other flavonoids, e.g., apigenin, isorhamnetin glycosides, sakuranetin, and sakuranin, may facilitate the adaptation of *C. officinarum* for protective purposes against adverse environmental conditions. These findings lay a theoretical foundation for resource exploration and the ornamentation improvement of *C. officinarum*.

Keywords: *Camphora officinarum*; flavonoid biosynthesis; integrated omics analysis

check for updates

Academic Editor: Carol A. Loopstra

Received: 29 July 2025
Revised: 12 September 2025
Accepted: 17 September 2025
Published: 19 September 2025

Citation: Peng, X.; Xie, P.; Li, B.; Zhong, Y.; He, B.; Wang, Y.; Chen, Y.; Li, N.; Hou, C. Integrated Transcriptome and Metabolome Analysis Reveals Molecular Mechanisms of Flavonoid Biosynthesis During *Camphora officinarum* Leaf Development. *Forests* **2025**, *16*, 1490. https://doi.org/10.3390/f16091490

Copyright: © 2025 by the authors. Licensee MDPI, Basel, Switzerland. This article is an open access article distributed under the terms and conditions of the Creative Commons Attribution (CC BY) license (https://creativecommons.org/licenses/by/4.0/).

1. Introduction

Camphora officinarum Nees, a vital evergreen broad-leaved species within subtropical forest ecosystems, is extensively distributed in regions south of the Yangtze River Basin. It holds significant ecological, economic, and medicinal importance [1]. With its broad crown and dense branches and leaves, *C. officinarum* can effectively sequester carbon, release oxygen, conserve water sources, absorb smoke, and trap dust. It also has strong resistance to toxic gases, making it an optimal tree species for urban landscaping and ecological restoration [2–4]. As a versatile economic tree, its timber is prized for its bright color, resistance to decay and insects, and fine grain, making it eminently suitable for the creation of high-end furniture and intricate carving crafts [5]. Furthermore, various parts of the tree—including the bark, roots, stems, leaves, and fruits—contain valuable

components such as essential oils, camphor, and linalool. These components can be extracted to produce natural essential oils, which impart a distinct aroma and exhibit notable antibacterial, anti-inflammatory, and antioxidant activities [6,7]. Consequently, they are widely used in traditional medicine, daily chemicals, and biological pest control [8,9]. Modern pharmacological research has further confirmed that extracts from *C. officinarum* possess diverse biological activities, including insect repellent, antiseptic, antibacterial, antitumor, and cardiovascular protective effects. These properties are closely associated with its complex phytochemical composition [10]. Particularly importantly, besides volatile components like terpenoids, *C. officinarum* leaves are also rich in non-volatile medicinal active substances such as flavonoids [11,12]. Flavonoids, a class of polyphenolic secondary metabolites ubiquitous in the plant kingdom, are predominantly accumulated in flowers, fruits, and leaves, demonstrating distinct tissue-specific distribution patterns [13]. They can be classified into seven major subclasses: chalcones, flavones, flavonols, flavanones, flavanols, isoflavones, and anthocyanins [14]. These compounds not only contribute to the vivid coloration of floral and fruit tissues but also play crucial roles in plant growth, development, and stress responses [15]. At the same time, due to their strong effects of antioxidation and anti-inflammation, anti-cancer, and cardiovascular protection, they make important contributions to human health [16,17]. The biosynthetic pathway is primarily composed of phenylpropanoid metabolism and the flavonoid branch pathway, involving the participation of various key structural genes, such as phenylalanine ammonia-lyase (*PAL*), chalcone synthase (*CHS*), chalcone isomerase (*CHI*), and flavanone 3-hydroxylase (F3H), among others. In addition, the coordinated expression of the structural genes is usually regulated by a complex of transcription factors, including MYB, bHLH, and WD40 repeat proteins individually or coordinately [18–20].

Interestingly, current research on *C. officinarum* has primarily focused on the extraction of volatile oils, the investigations into pharmacological activities, and the exploration and functional verification of terpene synthase genes. However, there remains a significant gap in research on leaf development processes, especially the synthesis and regulatory network of flavonoids that accompany the succession of developmental stages. It is noteworthy that leaf development is a highly coordinated and complex biological process, involving the precise regulation of gene expression and the dynamic reconstruction of metabolic networks. These processes ultimately determine the physiological functions of leaves and the accumulation of secondary metabolites [21,22]. As an important ecological and economic tree species, the synthesis and accumulation of flavonoids in *C. officinarum* leaves are inevitably subject to dynamic regulation throughout their life cycle, from juvenility to maturity and senescence. Several critical questions arise: What molecular mechanisms can comprehensively delineate the expression patterns of flavonoid biosynthesis genes and their corresponding metabolites during the various developmental stages of *C. officinarum* leaves? Which transcriptional regulators might govern the expression of these structural genes, thereby influencing the accumulation of flavonoids? What are the ecological and economic implications of the temporally specific patterns of flavonoid synthesis in *C. officinarum* leaves? In recent years, integrated multi-omics analysis has emerged as a powerful tool for deciphering the molecular mechanisms underlying complex biological processes. Transcriptomics provides a global view of gene expression profiles [23], while metabolomics depicts the composition and abundance dynamics of metabolites [24]. Integrative analysis of both datasets enables effective identification of key genes and regulatory factors driving specific metabolic phenotypes, revealing functional linkages between genes and metabolites, and thereby offering a more comprehensive understanding of the intrinsic mechanisms of biological processes. With advances in sequencing technologies, this integrated strategy has demonstrated significant advantages in elucidating growth and development, stress

responses, and regulation of specific secondary metabolic pathways in other plant species, providing profound insights into the molecular basis of complex traits [25–27]. Therefore, it is urgently necessary to adopt an integrated multi-omics approach to deeply analyze the coordinated variation patterns between flavonoid gene expression profiles and flavonoid metabolic profiles at different developmental stages of *C. officinarum* leaves. This will help fill the knowledge gap in this field and provide key evidence for revealing the molecular basis underlying the formation of the medicinal quality of *C. officinarum* leaves.

This study systematically investigated the dynamics of flavonoid biosynthesis in *C. officinarum* leaves across key developmental stages. Significant differences in flavonoid accumulation were observed among leaves at different developmental phases. Our primary objective was to elucidate the gene expression networks underlying the formation of stage-specific flavonoid metabolic profiles and to explore their adaptive significance during leaf development. To achieve this, we employed an integrated multi-omics analysis strategy. Transcriptome sequencing (RNA-Seq) provided a detailed atlas of gene expression related to flavonoid biosynthesis across various developmental stages, while non-targeted metabolomics based on ultra-high-performance liquid chromatography-tandem mass spectrometry (UHPLC-MS/MS) enabled comprehensive and accurate identification and quantification of flavonoids and related metabolites. These techniques allowed us to thoroughly analyze the dynamic changes in the flavonoid biosynthetic pathway during leaf development and to identify key regulatory nodes and network modules influencing this pathway. By deeply integrating transcriptomic and metabolomic data, we aimed to identify transcription factors, structural genes, and hub metabolic pathways regulating flavonoid synthesis in developing *C. officinarum* leaves. This understanding is essential for clarifying how *C. officinarum* modulates flavonoid production to meet developmental demands and fulfill its physiological and ecological functions. The findings of this study possess dual potential applications: at the basic research level, elucidating the mechanism linking leaf development and flavonoid synthesis in *C. officinarum* provides new insights into the developmental regulation of secondary metabolism in woody plants; at the applied level, the identified key genes and metabolic markers offer potential targets for molecular-assisted breeding aimed at developing superior varieties with specific flavonoid contents. Overall, this integrated study enhances our understanding of the mechanisms underlying leaf development and secondary metabolite synthesis in *C. officinarum* and highlights the crucial role of combined multi-omics analysis in deciphering the molecular mechanisms of complex biological processes.

2. Materials and Methods

2.1. Plant Materials

The experimental materials consisted of healthy mother plants of *C. officinarum* (strain LX3-23) collected from the hillside nursery of Guangdong Academy of Forestry Sciences, Guangdong Province, China, during April to May 2024 (23°16′ N, 113°37′ E). The nursery is situated in a subtropical monsoon climate zone, characterized by a mild climate, abundant heat resources, and sufficient rainfall. The annual average temperature is 19.3 °C, the annual average relative humidity is 77%, the annual rainfall is approximately 1600 mm, the annual sunshine duration is about 1600 h, and the frost-free period is no less than 300 days. The soil is predominantly acidic lateritic red earth, making these conditions well-suited for the growth of *C. officinarum*. Leaf samples were collected at 3 distinct developmental stages, including 7 days (S1), 14 days (S2), 21 days (S3). Triplicate biological samples were collected for every stage, resulting in a total of 9 samples. Transcriptome sample categorization: Group S1 has samples LZST11, LZST12, and LZST13; Group S2 includes LZST21, LZST22, and LZST23; Group S3 consists of LZST31, LZST32, and LZST33.

Metabolome sample categorization: Group S1 consists of LZSD11, LZSD12, and LZSD13; Group S2 includes LZSD21, LZSD22, and LZSD23; Group S3 comprises LZSD31, LZSD32, and LZSD33. Each replicate sample included 6 g of leaves, allocated for metabolomic profiling (2 g), transcriptomic analysis (2 g), and quantitative real-time polymerase chain reaction (qRT-PCR) validation (2 g). Immediately after collection, samples were wrapped in aluminum foil, sub-aliquoted, labeled, flash-frozen in liquid nitrogen, and stored at −80 °C until the following multi-omics analyses. The comprehensive experimental approach is depicted in Figure 1.

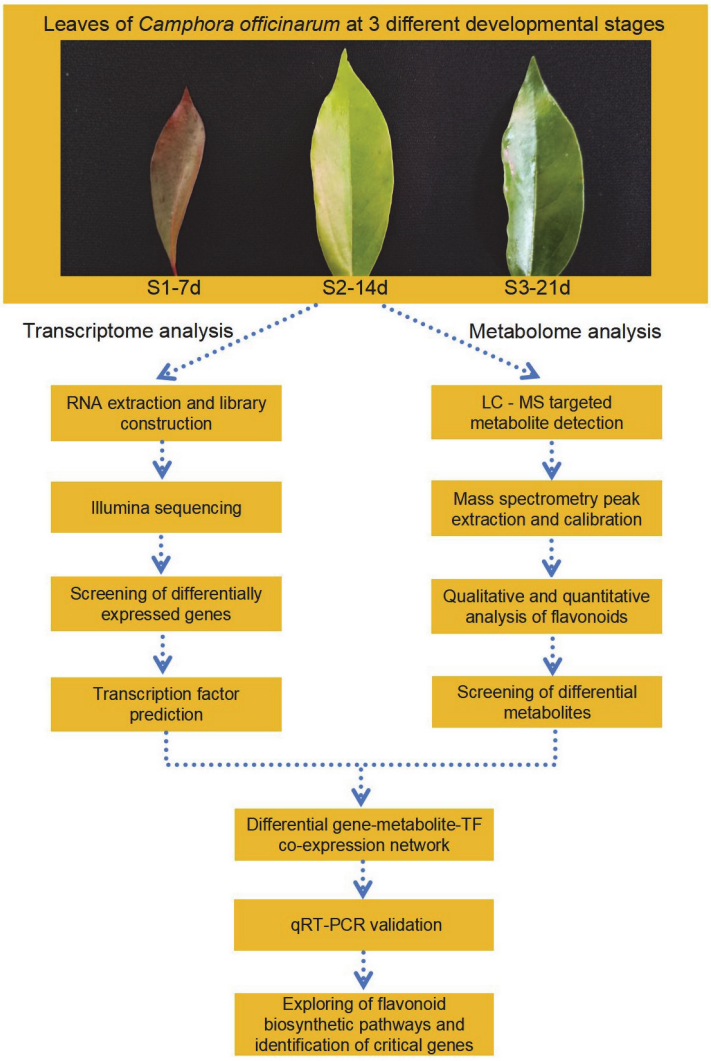

Figure 1. A technical workflow depicts integrated transcriptomic and metabolomic analysis of *C. officinarum* leaves at three developmental stages.

2.2. Targeted Metabolomics Profiling and Analysis

The protocol involved immediately freezing the 9 leaf specimens in liquid nitrogen, followed by lyophilization with a vacuum freeze-dryer (Scientz-100F, Ningbo Scientz Biotechnology Co., Ltd., Ningbo, China). Subsequently, the samples were pulverized into homogeneous powder using a grinder (MM 400, Retsch, Haan, Germany) operating at 30 Hz for 90 s. Exactly 100 mg of the lyophilized powder was blended with 1.2 mL of 70% methanol aqueous solution. The mixture was vortexed for 30 s and subsequently vortexed at 30 min intervals for 6 cycles, followed by 12–16 h of incubation at 4 °C. The samples were centrifuged at 12,000 rpm for 10 min, after which the supernatant underwent

filtration using a 0.22 μm microporous membrane (SCAA-104, ANPEL, Shanghai, China). The resulting filtrate (2 μL) was then subjected to UPLC-MS/MS analysis.

According to methods in Chen et al. with modifications, the method for detecting a variety of metabolites in the leaves of *C. officinarum* has been performed [28]. Chromatographic separation was achieved using an ultra-high-performance liquid chromatography system (UHPLC, SHIMADZU Nexera X2, Shimadzu Corporation, Kyoto, Japan), equipped with an Agilent SB-C18 reversed-phase column (2.1 mm × 100 mm, 1.8 μm). The mobile phase included water containing 0.1% formic acid (solvent A) and acetonitrile containing 0.1% formic acid (solvent B). The gradient elution program was set as follows: phase B increased linearly from 5% to 95% over 0~9 min, was maintained isocratically at 95% for 1 min, subsequently re-equilibrated to the initial composition over 1.1 min, and finally equilibrated for 2.9 min. The analytical method employed a column temperature of 40 °C, 0.35 mL/min flow rate, and 4 μL injection volume. Detection was performed using a triple quadrupole linear ion trap mass spectrometer (QTRAP 4500, AB Sciex, Framingham, MA, USA), equipped with an electrospray ionization (ESI) source operating in both positive and negative ion modes. The ESI source parameters were set as follows: ion spray voltage, ±5500 V; curtain gas (CUR), 25 psi; ion source gas I (GS1), 50 psi; ion source gas II (GS2), 60 psi; temperature, 550 °C. Data acquisition was conducted in multiple reaction monitoring (MRM) mode. Collision energy (CE) and declustering potential (DP) were optimized for each target metabolite.

2.3. Metabolite Identification, Quantification, and Differential Metabolite Screening

Metabolite annotation was performed on the basis of the Metware database (MWDB) and characteristic secondary mass spectrometry fragments [29]. Raw MS data were processed using Analyst 1.6.3 software for peak extraction, integration, and baseline correction [30]. Quantification of metabolites employed a combined strategy utilizing external standard calibration curves and internal standard normalization to minimize systematic errors. The selection of differential metabolites was performed according to 2 key criteria: a variable importance in projection (VIP) value ≥ 1 from the orthogonal projections to latent structures discriminant analysis (OPLS-DA) model, as well as a univariate analysis showing a significant change with a fold change (FC) ≥ 2 or ≤ 0.5 ($p < 0.05$). All bioinformatics analyses were performed using the MetaboAnalystR package (v.1.0.1) within the R statistical environment (v.3.5.1) [31]. All percentages of detected metabolites were calculated based on the total mass of detected metabolites in this study, rather than based on the number of substances in a group.

2.4. Total RNA Extraction and Library Construction

Total RNA was extracted from samples using the RNAprep Pure Plant Kit (DP441, Tiangen, China). Prior to sequencing, RNA quality underwent rigorous assessment through complementary approaches: purity determination using a NanoPhotometer spectrophotometer (IMPLEN, Westlake Village, CA, USA), concentration measurement with a Qubit 2.0 Fluorometer (Life Technologies, Carlsbad, CA, USA), and integrity evaluation on an Agilent Bioanalyzer 2100 system (Agilent Technologies, Santa Clara, CA, USA). Upon passing quality control, eukaryotic poly(A)+ mRNA was enriched with Oligo(dT) magnetic beads (Illumina, Inc., San Diego, CA, USA). The purified mRNA was fragmented (200–300 bp) via fragmentation buffer. First-strand cDNA synthesis employed random hexamer primers, followed by second-strand synthesis using buffer, dNTPs, and DNA polymerase I. Double-stranded cDNA was ligated to sequencing adapters using the NEBNext Ultra II DNA Library Prep Kit (New England Biolabs, Ipswich, MA, USA). Size selection (~200 bp fragments) was performed with AMPure XP beads (Beckman Coulter,

Brea, CA, USA). After PCR amplification and purification, libraries were constructed for high-throughput paired-end sequencing on the Illumina NovaSeq 6000 platform [32]. The raw sequencing data were deposited in the NCBI Sequence Read Archive (SRA) database under accession number PRJNA1287255.

2.5. Functional Annotation and Classification

Raw sequencing reads were subjected to stringent quality filtering using fastp (v.0.19.3) to gain relatively high-quality clean reads [33]. The filtering parameters employed were set as follows: a nucleotide base limit of 15 and a qualified quality Phred score of 20. These clean reads were then aligned to the *C. officinarum* reference genome sequence using HISAT2 (v.2.1.0), yielding mapped reads [34]. The mapping efficiency, calculated as the percentage of clean reads mapped against the reference genome, was utilized to assess transcriptome data utilization. To predict gene function, the sequences of all mapped reads were aligned against several databases using the Diamond procedure with an E-value threshold of 1×10^{-5} [35]. The databases included the NCBI Non-redundant protein database (NR, https://ftp.ncbi.nlm.nih.gov/blast/db/, accessed on 14 April 2025), Gene Ontology (GO, http://www.geneontology.org, accessed on 14 April 2025), Clusters of Orthologous Groups (COG, https://www.ncbi.nlm.nih.gov/COG/, accessed on 14 April 2025), and the Kyoto Encyclopedia of Genes and Genomes (KEGG, https://www.genome.jp/kegg, accessed on 15 April 2025), Swiss-prot protein database (Swiss-Prot, http://www.expasy.ch/sprot, accessed on 15 April 2025), and Protein family (Pfam, https://pfam.xfam.org/, accessed on 15 April 2025). This homology-based comparison identified high-similarity protein sequences to obtain functional annotations for the mapped reads.

2.6. Differential Expression Gene Screening

Gene expression levels were quantified using fragments per kilobase of transcript per million mapped reads (FPKM), computed via FeatureCounts (v.1.6.1) [36]. Differential expression analysis between the different developmental stages was performed using the DESeq2 package [37,38]. Following differential analysis, the Benjamini–Hochberg method was applied to adjust the *p*-values for multiple hypothesis testing, yielding the false discovery rate (FDR). DEGs with biological significance were identified using a dual-threshold criterion: absolute $\log_2$fold change ($|\log2FC|$) ≥ 1 and FDR < 0.05. To find significantly enriched biological pathways, the DEGs were subjected to hypergeometric testing based on KEGG database pathways by comparing against the whole genome of *C. officinarum*.

2.7. Transcription Factor Prediction and Weighted Gene Co-Expression Network Construction

To identify transcription factors (TFs) in *C. officinarum*, putative TF protein sequences were annotated against the Plant Transcription Factor Database (PlantTFDB v.4.02) using iTAK software (v.1.5) with an E-value threshold of 1×10^{-5} [39,40]. Based on the transcriptome-derived gene expression matrix, low-expression and invariant genes were filtered using the 'varFilter' function from the R genefilter package (v.3.5.1) [41]. The WGCNA package (WGCNAN v.1.71) was then applied to complete co-expression networks construction and identify gene modules [42], with parameters set as follows: soft-thresholding power = 18, merge cut height = 0.25, and minimum module size = 50. Subsequently, 12 key differentially accumulated flavonoids were selected from metabolomic data. Module-trait association analysis identified key gene modules significantly correlated with these target flavonoids. Pearson correlation analysis (stats package v.3.5.1) was performed to determine relationships between TFs and target genes, and between target genes and metabolite abundance ($|PCC| > 0.8$, $p < 0.05$) [43]. The TF–target gene–metabolite regulatory network was visualized using Cytoscape v3.10.3 [44].

2.8. Quantitative Real-Time PCR (qRT-PCR) Validation

RNA extraction was carried out from *C. officinarum* leaves representing 3 developmental stages. Equal amounts of total RNA (1 μg) per sample were reverse transcribed into complementary DNA (cDNA) using the HiScript III RT SuperMix for qPCR kit (Vazyme Biotech Co., Ltd., Nanjing, China), according to the manufacturer's instructions. The resulting cDNA products were stored on ice for immediate use or at −20 °C for subsequent analysis. These cDNA samples served as templates for qPCR reactions. Each 20 μL qPCR reaction mixture consisted of 10 μL ChamQ Universal SYBR qPCR Master Mix (Vazyme Biotech Co., Ltd., Nanjing, China), 1 μL cDNA, 0.4 μL each of forward and reverse primers, and 8.2 μL ddH_2O. After loading, reaction plates were briefly centrifuged to homogenize the mixtures and remove air bubbles. Amplification was performed on a CFX96 Touch Real-Time PCR Detection System (Bio-Rad, Hercules, CA, USA) using the following thermal cycling program: initial denaturation at 95 °C for 30 s, followed by 40 cycles of denaturation at 95 °C for 10 s and extension at 60 °C for 30 s. All primer sequences were designed using Primer 5 software and validated for specificity. The details pertaining to the primers utilized in the current study are presented in Table S1. Relative expression levels of target genes were calculated and normalized using the $2^{-\Delta\Delta Ct}$ method [45].

3. Results

3.1. Metabolomic Analysis

To investigate metabolic variations during leaf development, metabolite analysis at 3 developmental stages (S1, S2, and S3) was conducted through LC–MS/MS. Based on the total mass detection, a total of four hundred and fifty-seven metabolites were detected, containing one hundred and twenty-six phenolic acids (28%), one hundred and seventy-five flavonoids (38%), forty-four types of lignans and coumarins (10%), twelve tannins (3%), sixty-two alkaloids (13%), eight terpenoids (2%), and thirty others (6%) (Figure S1a). The analysis revealed that flavonoids, phenolic acids, and alkaloids were the predominant metabolites during leaf development of *C. officinarum*. The one hundred and seventy-five identified flavonoids were subsequently categorized into eighty-four flavonols (constituting 48%), thirty-three flavones (19%), seventeen flavanones (10%), fifteen flavonoid carbonosides (9%), fourteen flavanols (8%), eighteen chalcones (4%), and four flavanonols (2%), as depicted in Figure S1b. It is particularly noteworthy that the relative abundance of certain flavonoids, including quercetin-7-O-(6″-malonyl)glucoside, quercetin-3-O-(6″-O-malonyl)glucosyl-5-O-glucoside, kaempferol-3-O-(6″-malonyl) glucoside-7-O-glucoside, and kaempferol-3-O-(3″-O-p-coumaroyl)rhamnoside, was observed to be elevated in S1. Conversely, the relative abundance of isorhamnetin-3-O-rutinoside (Narcissin) and apigenin-7-O-rutinoside (Isorhoifolin) was found to be more pronounced in S3. These fluctuations in the content of the 175 flavonoids across the three distinct developmental stages were notably evident, as illustrated in Figure S2.

Prior to undertaking differential expression analysis, a principal component analysis (PCA) was executed to evaluate metabolic variations. The PCA plot indicated a clear distinction among the three developmental stages, with the first principal component (PC1, accounting for 58.31%) and the second principal component (PC2, accounting for 21.07%) together explaining 79.38% of the variance. Differential metabolites were identified by integrating fold change and variable importance in projection (VIP) values. In the comparison between LZSD1 and LZSD2, 222 metabolites displayed significant differences (149 upregulated, 73 downregulated), whereas 230 metabolites were differentially expressed in the comparison between LZSD1 and LZSD3 (144 upregulated, 86 downregulated). The comparison between LZSD2 and LZSD3 revealed 86 differential metabolites (47 upregu-

lated, 39 downregulated) (Figure 2a). Among these, 32 metabolites were common across all three comparisons, with 14 being flavonoid-related. Specifically, 88, 92, and 34 flavonoid-associated metabolites were identified in the comparisons between LZSD1 and LZSD2, LZSD1 and LZSD3, and LZSD2 and LZSD3, respectively.

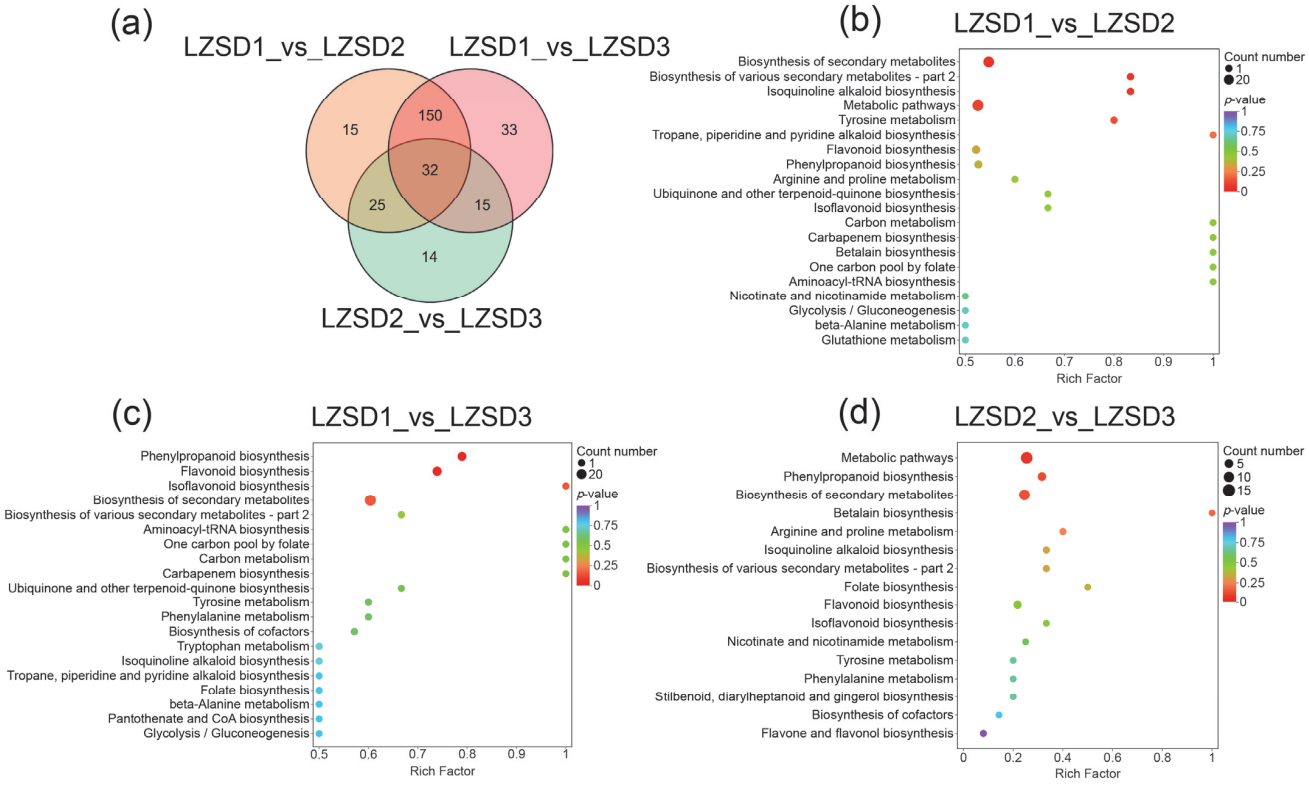

Figure 2. Analysis of the differential metabolome in leaves of *C. officinarum* at three developmental stages. (**a**) Venn diagram illustrating the differential metabolites across three distinct comparative groups: LZSD1 versus LZSD2, LZSD1 versus LZSD3, and LZSD2 versus LZSD3. (**b**–**d**) Bubble charts depicting the KEGG enrichment analysis results for the differential metabolites in the three comparative groups: LZSD1 versus LZSD2, LZSD1 versus LZSD3, and LZSD2 versus LZSD3. The vertical axis corresponds to the pathway names as listed in the KEGG database, while the horizontal axis represents the Rich factor values, with a higher Rich factor indicating a greater extent of enrichment. The color of the bubbles signifies the enrichment significance (*p*-value), where a deeper red color corresponds to a higher level of statistical significance. The size of the bubbles is proportional to the quantity of metabolites enriched within the specific pathway.

KEGG enrichment analysis categorized the differential metabolites into distinct pathways (Figure 2b–d). In the comparison of LZSD1_vs_LZSD2, fifty metabolites were ascribed to twenty-eight pathways, encompassing metabolic pathways (ko01100, with thirty-one metabolites), biosynthesis of secondary metabolites (ko01110, with twenty-nine metabolites), flavonoid biosynthesis (ko00941, with twelve metabolites), flavone and flavonol biosynthesis (ko00944, with eight metabolites), and phenylpropanoid biosynthesis (ko00940, with ten metabolites). In a similar vein, in LZSD1_vs_LZSD3, 59 metabolites were associated with 26 pathways, exhibiting significant enrichment in metabolic pathways (ko01100, with 30 metabolites), biosynthesis of secondary metabolites (ko01110, with 32 metabolites), flavonoid biosynthesis (ko00941, with 17 metabolites), flavone and flavonol biosynthesis (ko00944, with 12 metabolites), and phenylpropanoid biosynthesis (ko00940, with 15 metabolites). For LZSD2_vs_LZSD3, twenty-one metabolites were attributed to sixteen pathways, including metabolic pathways (ko01100, with fifteen metabolites), biosynthesis of secondary metabolites (ko01110, with thirteen metabolites), flavonoid

biosynthesis (ko00941, with five metabolites), flavone and flavonol biosynthesis (ko00944, with two metabolites), isoflavonoid biosynthesis (ko00943, with one metabolite), and phenylpropanoid biosynthesis (ko00940, with 6 metabolites). These results underscore the pivotal role of secondary metabolite biosynthesis, particularly within the flavonoid, flavone/flavonol, and phenylpropanoid pathways, during the process of leaf development.

3.2. Functional Annotation and Classification of DEGs

To elucidate the alterations in gene expression associated with flavonoids at various developmental phases of *C. officinarum* leaves, we chose leaves from three distinct stages (S1–7 d, S2–14 d, and S3–21 d) for sequencing analysis. Throughout the initial data quality assessment, sequences of inferior quality were culled, sequencing error rates were scrutinized, and the distribution of GC content was verified. Following the quality control measures, the filtered sequences ranged from 40,410,894 to 45,391,734, with the clean bases spanning 6.06–6.81 Gb (averaging 6 GB per sample). The alignment efficiency surpassed 90% in comparison to the *C. officinarum* reference genome sequence. Post-filtering base quality distributions met Q20 $\geq$ 96% (Phred $\geq$ 20) and Q30 $\geq$ 91% (Phred $\geq$ 30) (Table S2). These thorough quality metrics affirm the high reliability of the transcriptomic libraries for subsequent analyses.

The functional annotation of the acquired transcripts was executed through the integration of six authoritative databases, namely NR, Swiss-Prot, GO, KOG, KEGG, and Pfam. This process resulted in the identification of 29,491, 21,084, 24,220, 26,572, 20,473, and 22,658 annotated transcripts, respectively (Figure S3). Utilizing the NR database for GO analysis, 30,036 transcripts were categorized under molecular functions, with a significant concentration in binding (GO:0005488), catalytic activity (GO:0003824), and transporter activity (GO:0005215). Among the 68,084 transcripts associated with biological processes, cellular processes (GO:0009987), metabolic processes (GO:0008152), and responses to stimuli (GO:0050896) were the most prevalent. For cellular components, 81,258 transcripts were localized to the cell (GO:0005623), organelle (GO:0043226), and cell part (GO:0044464) (Figure S4). The KOG classification system partitioned 16,757 transcripts into 25 distinct categories, with the largest group being "General function prediction only" (3852), succeeded by "Posttranslational modification, protein turnover, chaperones" (1655), "Signal transduction mechanisms" (1469), and "Energy production and conversion" (1024) (Figure S5). Homology analysis conducted via the NR database unveiled species-specific divergence within the *C. officinarum* transcripts. The highest homology was observed with the lotus (*Nelumbo nucifera*, 6884 transcripts, 23.34%), followed by *Macleaya cordata* (3508, 11.9%), *Vitis vinifera* (1643, 5.57%), *Elaeis guineensis* (1325, 4.49%), and *Durio zibethinus* (1086, 3.68%). Notably, there were 8465 transcripts (28.7%) that lacked homology to known sequences (Figure S6).

3.3. Differential Expression Analysis of Expressed Genes

Principal Component Analysis (PCA) of nine RNA-seq samples revealed that the first principal component (PC1) accounted for 45.75% of the total variance, whereas the second principal component (PC2) contributed an additional 15.57%. Notably, significant distinctions were observed among all sample clusters, coupled with a high degree of reproducibility within each group. Utilizing FPKM values, a total of 28,772 genes were found to be expressed across three developmental stages, among which 8255 were identified as differentially expressed. Remarkably, 110 of these differentially expressed genes (DEGs) consistently demonstrated differential expression across all three stages, as depicted in Figure 3a. Stage-specific DEGs comprised 1163 unique to LZST1_vs_LZST2, 769 to LZST1_vs_LZST3, and 28 to LZST2_vs_LZST3. The comparison between LZST1 and LZST2

yielded the highest number of DEGs (7397), with 4843 genes downregulated and 2554 upregulated in relation to LZST1. Likewise, the comparison between LZST1 and LZST3 contained 7041 DEGs (4683 downregulated, 2358 upregulated), while LZST2_vs_LZST3 exhibited only 278 DEGs (89 downregulated, 189 upregulated). Hierarchical clustering heatmap analysis illustrated heterogeneous expression patterns of DEGs throughout the stages, with the most pronounced divergence observed between LZST1 and LZST2. The pronounced upregulation of DEGs in LZST1 suggests that this stage may be implicated in the flavonoid biosynthesis process during the leaf development of *C. officinarum*.

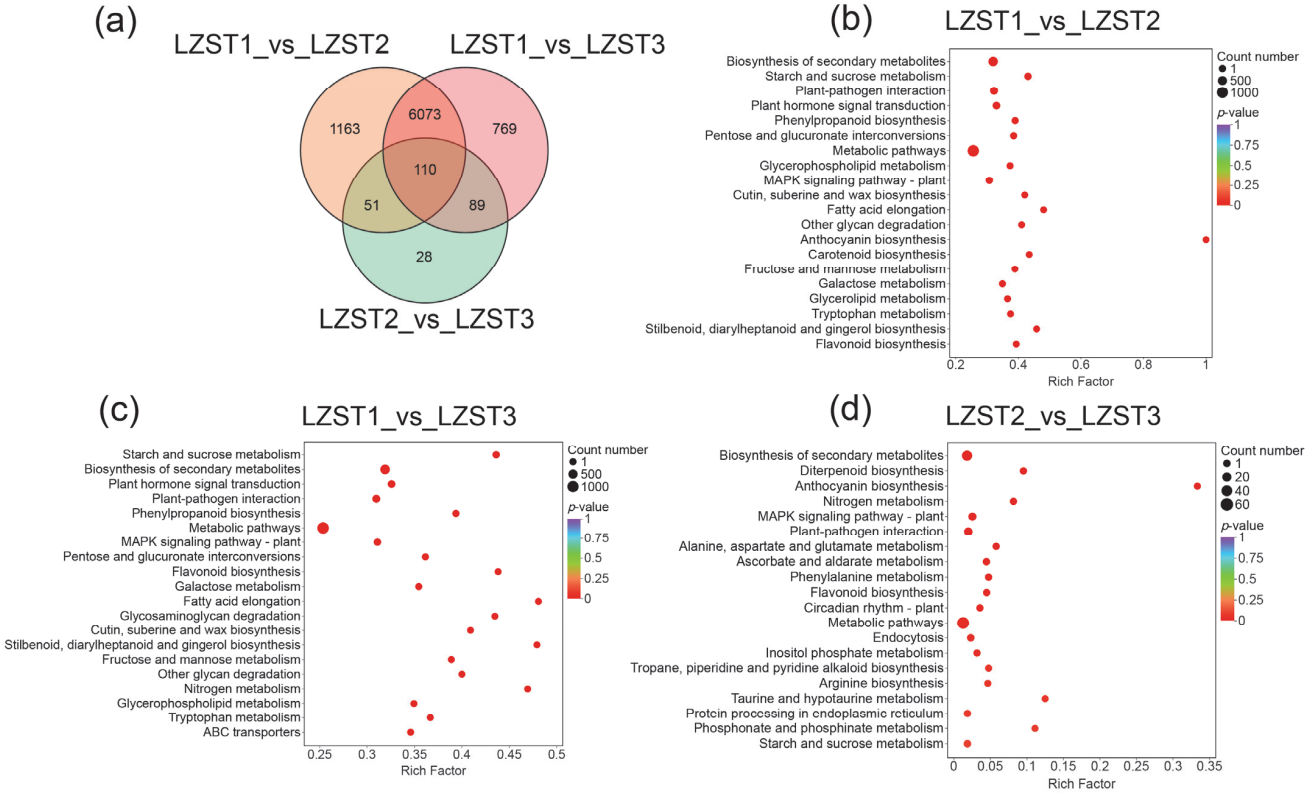

Figure 3. Analysis of the differential transcriptome in leaves of *C. officinarum* at three developmental stages: (**a**) Venn diagram illustrating the distribution of differentially expressed genes (DEGs) across three distinct comparison groups, namely LZST1_vs_LZST2, LZST2_vs_LZST3, and LZST1_vs_LZST3; (**b**–**d**) Bubble plots depicting the results of KEGG enrichment analysis for DEGs in the aforementioned comparison groups, LZST1_vs_LZST2, LZST2_vs_LZST3, and LZST1_vs_LZST3. The vertical axis corresponds to the pathway names as listed in the KEGG database. The horizontal axis signifies the Rich factor, with a higher value indicating a greater extent of enrichment. The color of the bubbles signifies the level of enrichment significance (*p*-value), where a deeper red hue corresponds to a higher statistical significance. The size of the bubbles is proportional to the quantity of genes that are enriched within the specific pathway.

To deduce the potential functions of differentially expressed genes (DEGs) throughout leaf development, a KEGG enrichment analysis was conducted on the top 20 significantly enriched pathways for each pairwise comparison among LZST1_vs_LZST2, LZST2_vs_LZST3, and LZST1_vs_LZST3 (refer to Figure 3b–d). During the transition from LZST1 to LZST2, the DEGs were predominantly associated with metabolic pathways (ko01100; 1205 genes), biosynthesis of secondary metabolites (ko01110; 705 genes), and plant–pathogen interaction (ko04626; 309 genes). Noteworthy flavonoid-related pathways encompassed phenylpropanoid biosynthesis (ko00940; 99 genes), flavonoid biosynthesis (ko00941; 35 genes), anthocyanin biosynthesis (ko00942; 6 genes), flavone/flavonol biosynthesis (ko00944; 5 genes), and isoflavonoid biosynthesis (ko00943; 13 genes). It

is particularly significant that the flavonoid biosynthesis pathways were most prominently enriched in LZST1_vs_LZST3, exhibiting comparable gene counts: phenylpropanoid biosynthesis (100 genes), flavonoid biosynthesis (39 genes), and isoflavonoid biosynthesis (13 genes). Conversely, the transition from LZST2 to LZST3 involved a lesser number of enriched DEGs. The pronounced enrichment of phenylpropanoid and flavonoid biosynthesis pathways in both LZST1_vs_LZST2 and LZST1_vs_LZST3 is consistent with the metabolomic data, whereas the plant–pathogen interaction pathway (ko04626) indicates the initiation of defense mechanisms starting from stage S1.

3.4. WGCNA Analysis

The application of weighted gene co-expression network analysis (WGCNA) to elucidate the mechanisms of flavonoid differential regulation throughout the developmental stages of *C. officinarum* leaves uncovered four gene co-expression modules with significant associations (Figure 4). The amalgamation of expression data from twelve principal flavonoids that differentially accumulated (Table S3), coupled with module eigengene correlation analysis, revealed that the MEblue module (comprising 4780 genes) and the MEturquoise module (encompassing 2463 genes) exhibited correlations of high statistical significance (with absolute correlation coefficients greater than 0.90 and *p*-values less than 0.05) with the majority of flavonoid metabolites. Additional analysis indicated that seven subclasses of flavonoids, including chalcones, flavones, and flavonols, displayed significant negative correlations with the MEblue module, yet positive correlations with the MEturquoise module. It is particularly noteworthy that the core structural genes involved in flavonoid biosynthesis were predominantly concentrated within the MEturquoise and MEblue modules. Subsequent research concentrated on these two modules. Remarkably, these genes exhibited distinct stage-specific expression patterns: Genes within the MEturquoise module were highly expressed during the early developmental stage (S1), coinciding with increased flavonol accumulation at S1, whereas genes within the MEblue module were markedly upregulated during the late developmental stage (S3). The outcomes of the WGCNA analysis facilitate a more profound exploration of key differentially expressed genes (DEGs) associated with flavonoid biosynthesis throughout the leaf development of *C. officinarum*.

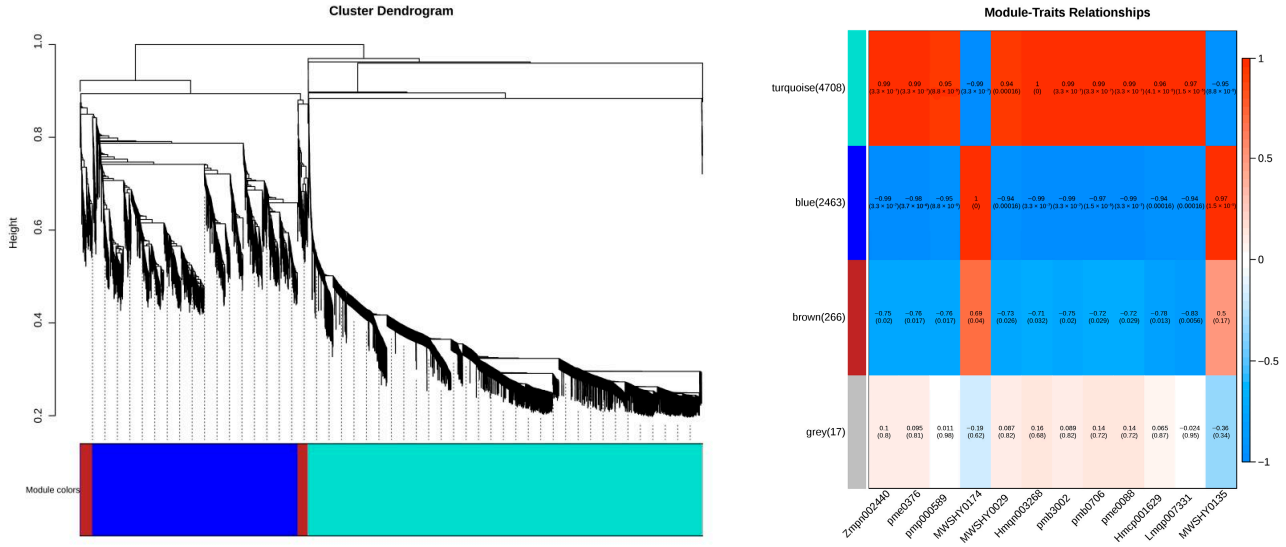

(**a**) (**b**)

Figure 4. Co-expression analysis of flavonoids and structural genes based on WGCNA. (**a**) Cluster dendrogram of metabolite-gene co-expression modules. The vertical axis represents the cluster tree

height, which signifies the distance metric between genes, whereas the horizontal axis delineates distinct gene co-expression modules, each color-coded to a specific module. (**b**) Heatmap of module–trait correlations. The numerical values within each square denote the correlation coefficients and associated *p*-values between modules and traits, with more intense colors indicating a greater absolute correlation.

3.5. Flavonoid Biosynthetic Pathways Analysis

Upon conducting a Weighted Gene Co-expression Network Analysis (WGCNA), the differentially expressed genes (DEGs) within the MEturquoise and MEblue modules were subjected to further scrutiny to identify genes associated with flavonoid metabolism during the leaf development of *C. officinarum*. Initially, a correlation network analysis was performed on these 25 DEGs in relation to 12 significantly accumulated flavonoid compounds across stages S1 to S3, employing a threshold greater than 0.8. Upon examination of the correlation analysis results, it has been identified that 25 distinct genes exhibit differential expression, which corresponds to 12 enzymes involved in the biosynthesis of flavonoids. A heatmap was subsequently generated to illustrate the differential expression of these genes within the established flavonoid biosynthetic pathway in the leaves of *C. officinarum* (Figure 5).

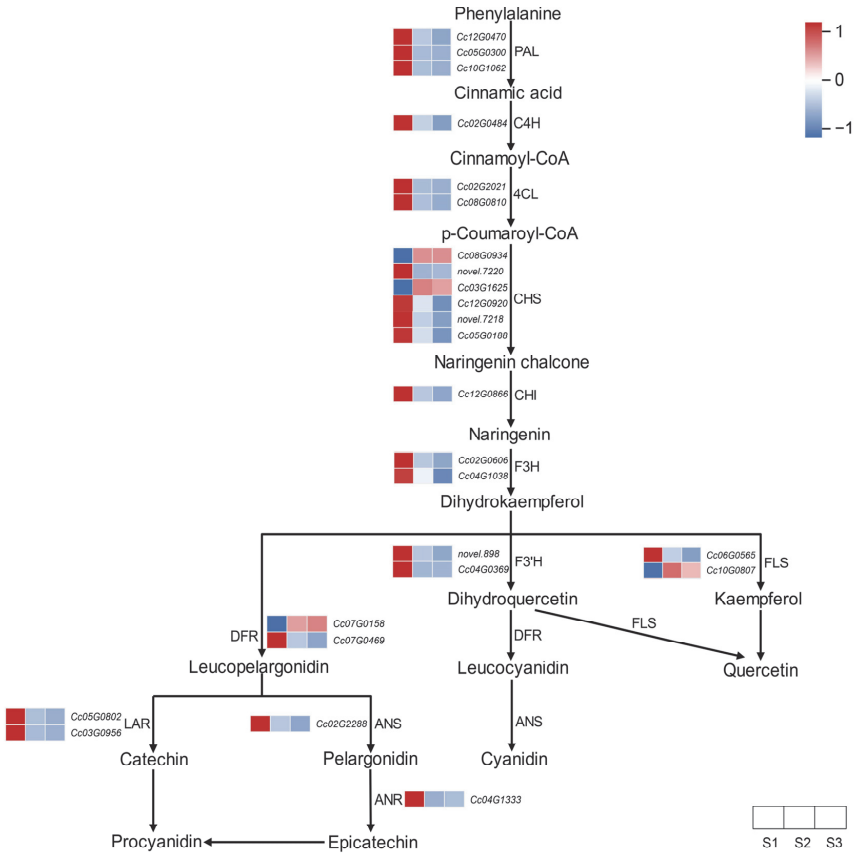

Figure 5. Expression analysis of DEGs involved in the flavonoid biosynthesis pathway in *C. officinarum* leaves. From left to right, the columns represent gene expression levels at S1, S2, and S3 stages, respectively. The analyzed genes include PAL (Phenylalanine ammonia-lyase), C4H (trans-cinnamate 4-monooxygenase), 4CL (4-Coumarate:CoA ligase), CHS (chalcone synthase), CHI (chalcone isomerase), DFR (dihydroflavonol 4-reductase), ANS (anthocyanidin synthase), F3′H (flavonoid 3′-hydroxylase), FLS (flavonol synthase), F3H (flavanone 3-hydroxylase), LAR (leucoanthocyanidin reductase), and ANR (anthocyanidin reductase).

The schematic delineates the critical enzymatic processes from phenylalanine to the final flavonoid products, such as procyanidin and epicatechin. At the initial activation

phase of the pathway, genes *PAL* (*Cc12G04740*) and *4CL* (*Cc05G05934*) exhibit a consistent upregulation across the samples, thereby propelling the metabolic flux into the pathway. *F3′H* (*Cc06G05655*) and *FLS* (*Cc10G06087*) demonstrate elevated expression levels during stages S2 and S3, which favors the production of kaempferol and quercetin. Regarding branch-specific regulation, the significant upregulation of *F3H* (*Cc02G0606*, *Cc04G1038*) and *F3′H* (*Cc04G0369*, *novel*.8189) enhances the hydroxylation of the flavonoid backbone, potentially facilitating the accumulation of flavonols, including quercetin and kaempferol. In the synthesis of proanthocyanidins, *DFR* (*Cc07G04698*) and *ANS* (*Cc03G09560*) reach peak expression levels in stage S1, steering carbon flow towards procyanidins. Interestingly, the high expression of *FLS* in stage S1 facilitates the conversion of flavanonols to flavonols, directly increasing the levels of quercetin and kaempferol, while competitively suppressing anthocyanin synthesis due to the low expression of *DFR*. During stage S1, the marked upregulation of *ANS* (*Cc02G2288*), *ANR* (*Cc04G1333*), and *LAR* (*Cc05G0802*, *Cc03G0956*) promotes the conversion of anthocyanins into leucoanthocyanidins and subsequently into proanthocyanidin monomers, such as catechin and epicatechin.

3.6. qRT-PCR Validation of Flavonoid Biosynthetic Genes

The outcomes presented above led to the identification and selection of nine structural genes involved in flavonoid biosynthesis for validation using quantitative polymerase chain reaction (qPCR). The experimental outcomes indicated a high level of concordance between the RNA sequencing (RNA-seq) and qPCR data (Figure 6a). A linear regression equation ($y = 0.005190x + 0.008634$) formulated for all ten genes exhibited a robust coefficient of determination ($R^2 = 0.9125$, Figure 6b). This validation of the transcriptional profiles confirms the technical reproducibility of the RNA-seq dataset and establishes a solid basis for subsequent analysis of gene expression patterns.

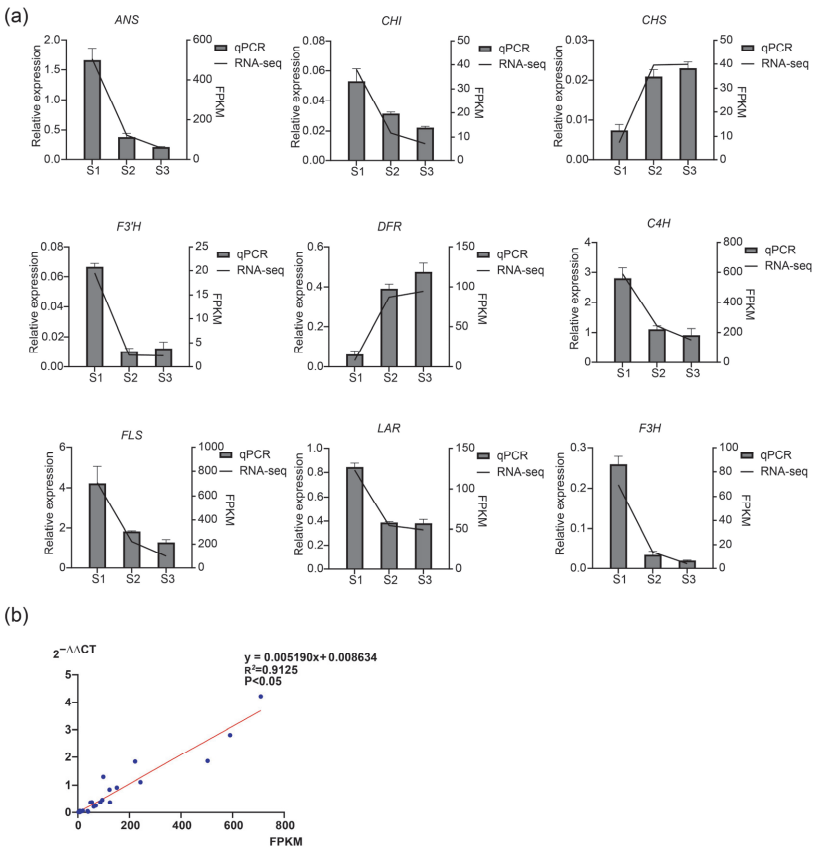

Figure 6. Analysis of the expression levels of nine flavonoid structural genes via quantitative reverse transcription polymerase chain reaction (qRT-PCR). (**a**) Bar graphs illustrating the expression levels

of eight pivotal structural genes in the leaves of *C. officinarum* at three distinct developmental stages (S1, S2, and S3). The black bars represent the qRT-PCR results (mean ± standard deviation, n = 3), which have been normalized against reference genes and are expressed as $2^{-\Delta\Delta CT}$ values. The lines depict the corresponding RNA sequencing data, expressed as fragments per kilobase of transcript per million mapped reads (FPKM), for comparative purposes. (**b**) A scatter plot delineating the linear correlation (depicted by the red dashed line) between the qRT-PCR ($2^{-\Delta\Delta CT}$, y-axis) and RNA-seq (FPKM, x-axis) measurements.

3.7. Gene–Metabolite Correlation Analysis

To substantiate the 25 key differentially expressed genes (DEGs) in relation to flavonoid biosynthesis, a correlation analysis was conducted, integrating all 175 identified flavonoids categorized into six groups with the 25 DEGs (Figure 7a,b). The findings indicated that the initial synthetic genes, such as *PAL*, *C4H*, *4CL*, and *CHS*, exhibited pronounced positive correlations with the accumulation of flavanones and flavones. Notably, various members of the *CHS* gene family demonstrated strong positive correlations with chalcones and flavonols. In contrast, the relationships between *DFR* and *LAR* with flavonols and flavonoid carbonosides were more complex, with some *DFR* and *LAR* genes showing negative correlations with these compounds. As key enzymes in flavonol synthesis, *F3H* and *FLS* exhibited significant positive correlations with the accumulation of flavonols, particularly at the S1 stage. *ANS* and *ANR* displayed positive correlations with specific flavonols and flavonoid carbonosides, suggesting their potential involvement in the synthesis or modification of flavonol-related compounds, especially during the later stages of development. The results of the Mantel test underscored a significant temporal correlation between the expression patterns of flavonoid biosynthesis genes and the accumulation of six major classes of flavonoid compounds throughout the leaf development of *C. officinarum*.

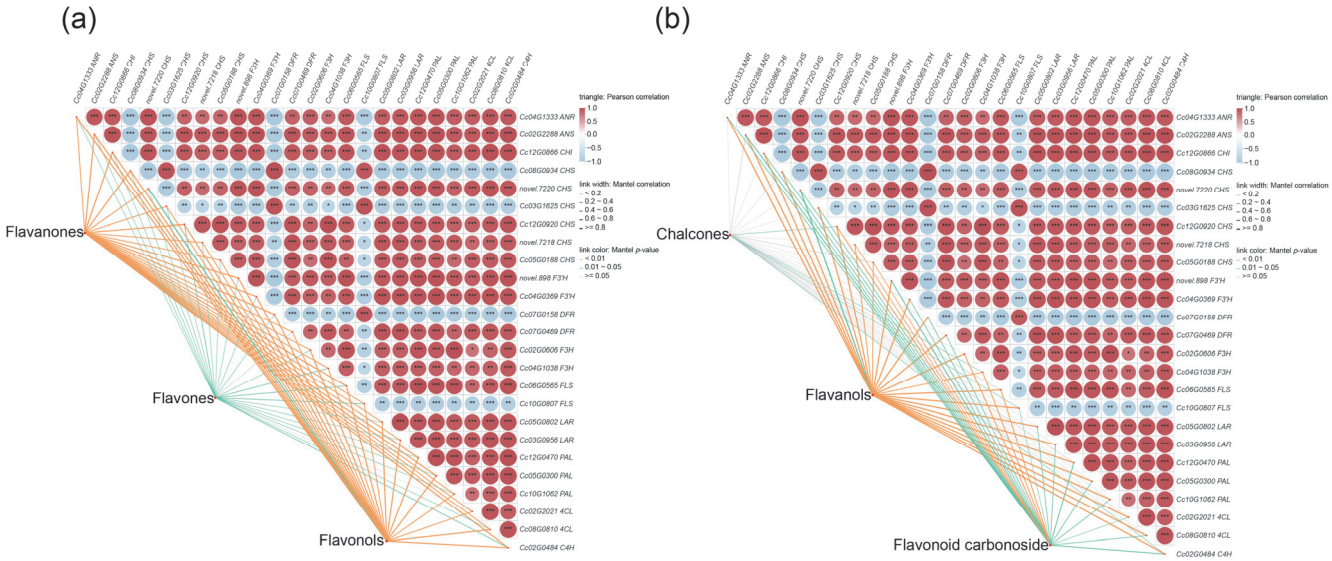

Figure 7. Mantel test analysis of the relation between genes and six categories of metabolites. (**a**) Mantel test analysis of the relation between 25 flavonoid genes and flavanones, flavones and flavonols. (**b**) Mantel test analysis of the relation between 25 flavonoid genes and chalcones, flavanols and flavonoid carbonoside. (The thickness of connecting lines indicates the magnitude of correlation coefficients, while line color represents the statistical significance of correlations. Red triangular areas denote positive correlations, blue areas indicate negative correlations, with *** $p < 0.001$, ** $p < 0.01$, and * $p < 0.05$).

3.8. Transcription Factor Analysis

Upon conducting a thorough analysis of transcriptomic data with the aid of a plant transcription factor database, we ascertained the presence of 51 transcription factor families, encompassing a total of 1942 potential transcription factors. The transcription factor families with the highest representation were as follows: 132 MYB, 132 members of AP2-ERF, 109 members of bHLH, 107 NAC, and 87 C2H2 (refer to Figure 8a). Comparative analyses of RNA-seq data across the LZST1_vs_LZST2, LZST2_vs_LZST3, and LZST2_vs_LZST3 groups unveiled 70, 71, and 16 differentially expressed transcription factors, respectively. The outcomes indicated that MYB, bHLH, and ERF transcription factors experienced a significant increase in expression at the S1 stage, which was subsequently followed by a pronounced decrease in expression during the S2 and S3 stages (Figure 8b). To delve deeper into transcription factors associated with flavonoid biosynthesis, 19 MYBs, 17 bHLHs, and 16 ERFs were pinpointed. The correlation analyses conducted among differentially expressed metabolites, target genes, and transcription factors, with a threshold exceeding 0.97, revealed ten MYBs, seven bHLHs, and three ERFs that correlated with twenty-five target differentially expressed genes and twelve significantly differentially expressed flavonoids (Figure 9). Notably, *CHS*, *FLS*, and *DFR* were identified as the core differential genes that govern metabolic flux allocation and product spectrum formation during flavonoid metabolism in the developmental stages of *C. officinarum* leaves.

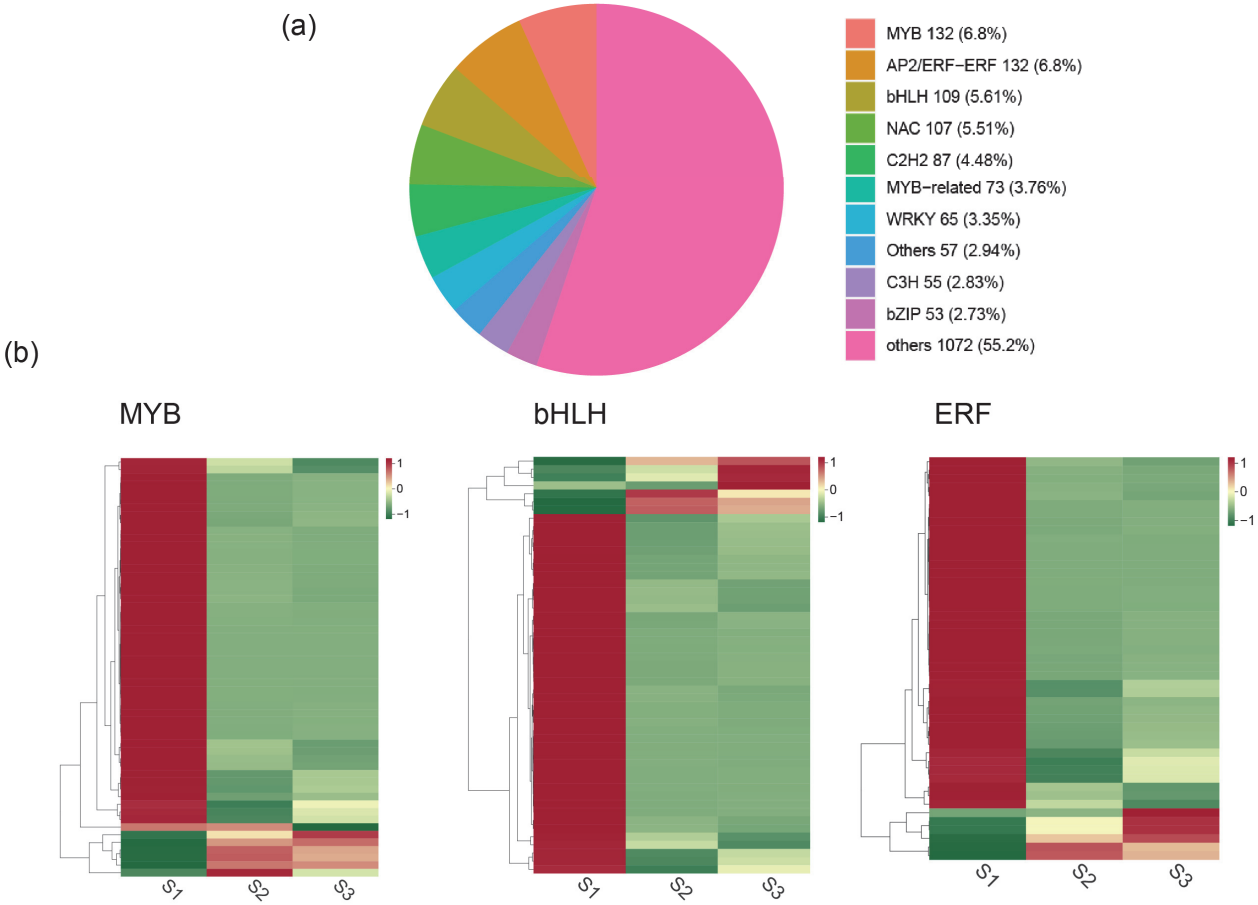

Figure 8. Classification and cluster analysis of transcription factors associated with flavonoid biosynthesis across three developmental stages. (**a**) Classification of transcription factors. (**b**) Comprehensive cluster analysis and heatmap depicting the expression patterns of MYB, bHLH, and ERF transcription factors across three developmental stages.

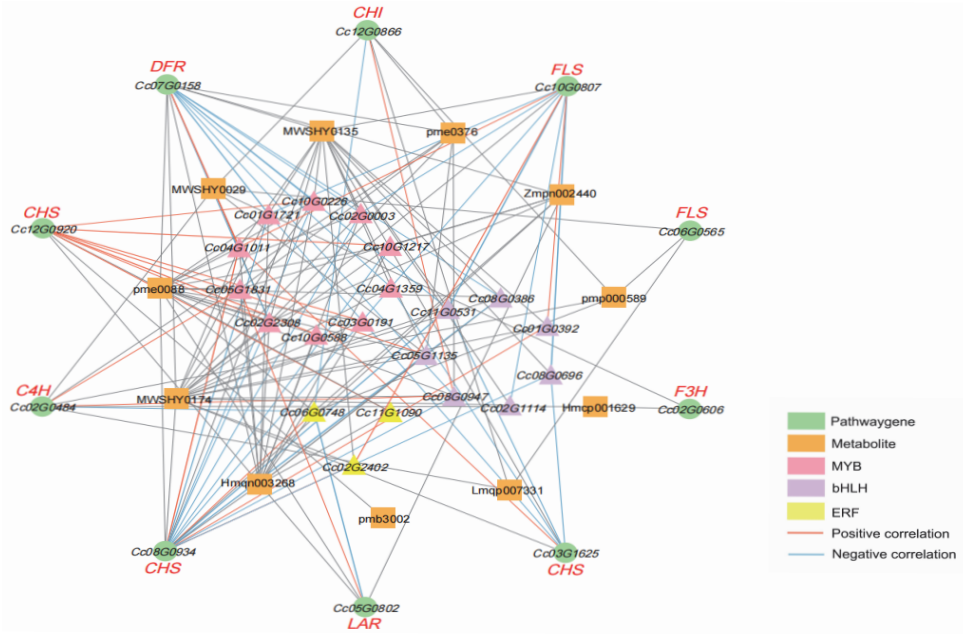

Figure 9. Interaction network of flavonoid biosynthesis genes, metabolites, and MYB/bHLH/ERF transcription factors (green nodes represent differentially expressed genes, orange nodes indicate differential metabolites, while pink, purple, and yellow nodes denote MYB, bHLH, and ERF transcription factors, respectively).

4. Discussion

This study incorporates three scientific questions related to flavonoid biosynthesis in *C. officinarum*. First, what molecular mechanisms delineate the expression patterns of flavonoid biosynthesis genes and metabolites during *C. officinarum* leaf development? Second, which transcriptional regulators govern the expression of structural genes and affect flavonoid accumulation? Third, what are the ecological and economic implications of the temporal patterns of flavonoid synthesis in *C. officinarum* leaves? To answer these questions, transcriptomic and metabolomic analyses were used to clarify the stage-specific regulatory network of flavonoid biosynthesis during *C. officinarum* leaf development (S1–S3). The findings show a sophisticated spatiotemporal coordination of structural genes, metabolic flux redirection, and transcription factor regulation, optimizing flavonoid diversity for *C. officinarum*'s development and environmental adaptation.

The investigation uncovered a significant disparity in the accumulation of particular flavonoid derivatives between the red and green leaves of *C. officinarum*. It is particularly noteworthy that the glycosides of kaempferol and quercetin, such as quercetin-3-O-rutinoside (rutin), quercetin-3-O-galactoside (hyperoside), quercetin-3-O-glucoside (isoquercitrin), kaempferol-3-O-rutinoside (nicotiflorin), and kaempferol-3-O-glucoside (astragalin), exhibited markedly elevated levels of accumulation in the red leaves in contrast to their green counterparts. This metabolic pattern suggests that these compounds are critical contributors to the coloration of the leaves, indicating a mechanism that differs from the conventional anthocyanin-mediated pigmentation process. Accordingly, by investigating the genetic basis of flavonoid biosynthesis during leaf development of *C. officinarum*, our differential gene expression analysis revealed a significant temporal accumulation pattern of flavonoids across developmental stages S1, S2, and S3. Notably, the expression of key upstream genes in this pathway—including *PAL*, *C4H*, *4CL*, *CHS*, *CHI*, and *F3H*—was highly expressed at stage S1 (Figure 5). This comprehensive activation of upstream genes provided ample substrates for the extensive synthesis of flavonoid skeletons from phenylalanine to dihydrokaempferol. Dihydrokaempferol is subsequently utilized in the biosynthesis

of various flavonoids, including procyanidin, cyanidin, and quercetin. The expression levels of genes *DFR* (*Cc07G0469*), *FLS* (*Cc06G0565*), *F3′H* (*novel. 898*, *Cc04G0369*), and *LAR* (*Cc05G0802*, *Cc03G0956*) were high at stage S1 (Figure 5). These genes are most likely to participate in pigmentation production at the early developmental stage of leaves in *C. officinarum*. Among these differentially expressed genes, *CHS*, *DFR*, *FLS*, *ANS*, and *LAR* genes draw our great attention. This is because it is a key gene that determines the color of the leaf. A previous study showed that *PbCHS1*, *PbCHS3*, and *PbCHS4* were highly expressed in the red-leaf stage (S1) of *Phoebe bournei*, positively correlating with cyanidin-3-O-glucoside levels. However, in later stages (S3), upregulation of *PbFLS* competitively diverted flavanonols from anthocyanin biosynthesis, leading to leaf greening [46]. The genes *CHS*, F3′H, *FLS*, *ANS*, *DFR*, and *LAR* related to flavonoid synthesis could have pivotal functions in the distinctions of flavonoid metabolism, causing the dynamic alterations of flavonoids in the red and green leaves of *Populus*×*euramericana* 'Zhonghuahongye' [47]. The concentrations of flavonoid metabolites in purple and green leaves were significantly affected by the genes (e.g., *CHS*, *FLS*, *LAR*, *DFR*) related to flavonoid biosynthesis in the 'Zijuan' tea plant cultivar [48]. In the pigmentation of a *Cinnamomum camphora* (=*C. officinarum*) red bark mutant ('Gantong 1'), a total of 25 upregulated DEGs encoding 11 enzymes (e.g., *CHS*, *F3′H*, *DFR*, *ANS*, *LAR*) were identified as key structural genes involved in anthocyanin biosynthesis [49]. Consequently, the outcomes of preceding studies corroborate that the color alterations of the leaves from S1 to S3 can be attributed to the differentially expressed flavonoid-related genes in *C. officinarum*.

In order to deeply understand the molecular mechanisms that drive the color changes during leaf development of *C. officinarum*, differentially expressed TFs were investigated. Our results show that ten MYBs, seven bHLHs, and three ERFs showed significant positive or negative correlations (>0.97) with the target genes, i.e., *CHS*, *DFR*, *LAR*, *F3H*, *CHI* and *C4H* (Figure 9). In *Ipomoea batatas* '*Purple Heart*', IbMYB1 functions as a key transcriptional regulator determining tuber flesh pigmentation, with its expression exclusively localized to the purple flesh tissues [50]. During leaf color change in *C. officinarum*, the homolog of MYB90 was specifically highly expressed, significantly upregulating the anthocyanin pathway genes *ANS* and *UFGT*, thereby driving anthocyanin accumulation and leaf pigmentation [51]. In *L. coreana*, LcsMYB123 was confirmed as a positive regulator, with its conserved R2R3 domain directly binding to the promoters of *CHS*, *F3H*, and *FLS* to promote the synthesis of flavonol derivatives such as quercetin and kaempferol [52]. Members of the bHLH family, including stress-responsive CbbHLH147 in *Camphora bodinieri* and PbbHLH1/2 in *P. bournei*, were found to positively regulate key genes such as *CHS*, *DFR*, *UGTs*, and *F3′H*, thereby enhancing the biosynthesis and accumulation of flavonoids, flavonols, and anthocyanins [46,53]. Another instance indicates that six transcription factors (three MYBs and three bHLHs) could be potential regulators of the anthocyanin biosynthesis pathways in the red and green stems of *C. officinarum* in 'Gantong 1' [49]. The biosynthesis of plant flavonoids is modulated not only by structural genes but also by the transcriptional activity of MYB, bHLH, and WD40 TFs, as well as the MBW complex [54,55]. In addition, ERFs exhibit complex regulatory roles in the anthocyanin biosynthetic pathway. In *Litchi chinensis*, the silencing of genes *LcERF1/22/25/37* notably inhibited the expression of anthocyanin biosynthetic genes and the accumulation of pigments. In contrast, the silencing of gene *LcERF64* exerted the opposite effect, facilitating pericarp coloration [56]. Another case shows that citrus ERF transcription factor CsERF003 was identified as a flavonoid activator in citrus fruit through integrated transcriptome and metabolome analysis [57]. The AP2/ERF transcription factor OfERF2 enhances flavonoid production in the petals of *Osmanthus fragrans* [58]. In *Cinnamomum cassia*, ERF2 showed a strong positive correlation with *F3H2* and *FLS1* expression, suggesting its core regulatory function

in flavonoids synthesis [59]. This evidence corroborate that members of the ERF family may exert bidirectional or context-dependent regulation within the flavonoid/anthocyanin metabolic pathway in *C. officinarum*. Thus, the up/down regulation of MYB, bHLH, and ERF TFs may influence color transition and flavonoid biosynthesis during leaf development of *C. officinarum.*

In addition to pigment production, alterations in the composition of flavonoid compounds during leaf development may facilitate the adaptation of *C. officinarum* for protective purposes against adverse environmental conditions. The present investigation utilized HPLC-MS/MS analysis to ascertain the composition and relative abundance of flavonoids in the leaves of *C. officinarum* at three distinct developmental stages. A total of 175 flavonoid compounds were identified, with flavonols (constituting 48%) and flavones (19%) emerging as the predominant subclasses, succeeded by flavanones (10%) and flavanols (8%). Despite the notable variations in their composition, the findings align with those reported for other medicinal plants, such as *Eucommia ulmoides*, *Hippophae rhamnoides* [60,61]. During the development of leaves, the accumulation patterns of specific flavonoids displayed distinct trends. The concentrations of quercetin and kaempferol glycosides experienced a gradual decline as the leaves matured, whereas the levels of isorhamnetin glycosides and apigenin exhibited a progressive increase, contributing to the dynamic shifts in composition throughout the developmental stages. Of particular interest, several flavonoids with established bioactivities were identified, including sakuranetin, sakuranin, phloretin, phlorizin, hesperetin, and hesperidin. Sakuranetin and sakuranin possess antitoxin properties [62], while phloretin and phlorizin have potential as biopesticides due to their effectiveness against pests, pathogens, and weeds [63,64]. Hesperetin and hesperidin exhibit pronounced antioxidant and anti-inflammatory properties [65]. Consequently, it is advised that the harvesting of young leaves (S1) be prioritized to maximize the yield of quercetin and kaempferol derivatives, while mature leaves (S3) are more appropriate for the extraction of sakuranetin/sakuranin, phloretin/phlorizin, and hesperetin/hesperidin. It is important to note that flavonoids from other members of the Lauraceae family, such as *Cinnamomum osmophloeum* and *Litsea cubeba*, have also been demonstrated to possess antioxidant and anti-inflammatory characteristics [66,67]. Furthermore, flavonoid extracts from *Persea americana* seeds have shown potential as insecticides and antimicrobials [68]. These findings highlight the significant potential of *Cinnamomum officinarum* leaf flavonoids for a range of applications, including cosmetics (as antioxidant and anti-inflammatory components) and environmentally friendly biopesticides (as fungicides and insecticides).

5. Conclusions

An integrated multi-omics analysis of flavonoid biosynthesis across three developmental stages (S1, S2, and S3) in *C. officinarum* leaves has elucidated stage-specific disparities in the expression of flavonoid biosynthetic genes, accumulation of metabolites, and underlying molecular regulatory mechanisms, along with their adaptive significance. Transcriptome analysis identified 8255 differentially expressed genes (DEGs). Metabolomics analysis detected a total of 175 flavonoid compounds, with flavonols being the most abundant. Notably, the relative abundance of certain flavonoids, including quercetin-7-O-(6″-malonyl)glucoside, quercetin-3-O-(6″-O-malonyl) glucosyl-5-O-glucoside, kaempferol-3-O-(6″-malonyl)glucoside-7-O-glucoside, and kaempferol-3-O-(3″-O-p-coumaroyl)rhamnoside, was observed to be elevated in S1. In contrast, the relative abundance of isorhamnetin-3-O-rutinoside (Narcissin) and apigenin-7-O-rutinoside (Isorhoifolin) was more pronounced in S3. Weighted gene co-expression network analysis predicted that 25 key differentially expressed genes (DEGs) encoding *CHS*, *DFR*, *FLS*, *ANS*, *F3′H*, and *LAR* genes are involved in anthocyanins biosynthesis related to color changes

during leaf development. Importantly, ten MYB, seven bHLH, and three ERF transcription factors are potentially involved in regulating key genes, highlighting their significant roles in the color mechanisms of flavonoid biosynthesis. Other flavonoids, such as apigenin, isorhamnetin glycosides, sakuranetin, and sakuranin, may promote the adaptation of *C. officinarum* for protective functions against adverse environmental conditions. In summary, this study provides the first elucidation of the dynamic regulatory network governing flavonoid biosynthesis during camphor tree leaf development. These findings lay a theoretical foundation for resource exploration derived from camphor tree leaves and ornamentation improvement of *C. officinarum*.

Supplementary Materials: The following supporting information can be downloaded at: https://www.mdpi.com/article/10.3390/f16091490/s1, Figure S1: Proportions and classification of all metabolites (a) and 175 flavonoids (b) at three developmental stages of *C. officinarum*; Figure S2: The heatmap elucidates the abundance of a total of 175 flavonoids through cluster analysis; Figure S3: The number of transcripts annotated according to six databases; Figure S4: Gene Ontology classification of all transcripts; Figure S5: Classification bar chart of gene KOG annotation; Figure S6: Species classification statistics diagram of gene NR database alignment; Table S1: Information of primers used for qPCR analysis; Table S2: Quality of RNA sequencing for the three developmental stages of *C. officinarum* leaves; Table S3: 12 major differentially accumulated flavonoid substances for WGCNA analysis.

Author Contributions: X.P.: Software, Formal analysis, Investigation, Data curation, Writing—original draft. P.X.: Methodology, Validation, Resources, Visualization. B.L.: Software, Validation, Formal analysis. Y.Z.: Conceptualization, Data curation, Visualization. B.H.: Validation, Resources, Visualization. Y.W.: Conceptualization, Software. Y.C.: Software, Formal analysis. N.L.: Conceptualization, Supervision. C.H.: Conceptualization, Software, Investigation, Resources, Data curation, Writing—original draft. All authors have read and agreed to the published version of the manuscript.

Funding: This research was supported by the Technology Program from Forestry Administration of Guangdong Province (2022KJCX006 to Qian Zhang) and Guangdong Provincial Key Laboratory of Silviculture, Protection and Utilization (SPU 2025-02 to Chen Hou).

Data Availability Statement: The data supporting the conclusions of this article (raw RNA-Seq reads) are available in the National Center for Biotechnology Information (NCBI) Sequence Read Archive (SRA): PRJNA1287255.

Acknowledgments: We appreciate the technical support and collaborative discussions from my classmate Tanhang Zhang from Northeast Forestry University.

Conflicts of Interest: The authors declare no conflicts of interest.

References

1. Zheng, W.; Zeng, W.; Tang, Y.; Shi, W.; Cao, K. Species diversity and biogeographical patterns of Lauraceae and Fagaceae in northern tropical and subtropical regions of China. *Acta Ecol. Sin.* **2018**, *38*, 8676–8687. [CrossRef]
2. Zhong, Y.D.; Yang, A.H.; Li, Z.T.; Zhang, H.; Liu, L.P.; Wu, Z.X.; Li, Y.Q.; Liu, T.Y.; Xu, M.; Yu, F.X. Genetic diversity and population genetic structure of *Cinnamomum camphora* in South China revealed by EST-SSR markers. *Forests* **2019**, *10*, 1019. [CrossRef]
3. Meng, J.; Li, M.; Guo, J.; Zhao, D.; Tao, J. Predicting suitable environments and potential occurrences for *Cinnamomum camphora* (Linn.) Presl. *Forests* **2021**, *12*, 1126. [CrossRef]
4. Li, D.; Lin, H.Y.; Wang, X.; Bi, B.; Gao, Y.; Shao, L.; Zhang, R.; Liang, Y.; Xia, Y.; Zhao, Y.P. Genome and whole-genome resequencing of *Cinnamomum camphora* elucidate its dominance in subtropical urban landscapes. *BMC Biol.* **2023**, *21*, 192. [CrossRef]
5. Zhou, Y.; Yan, W.D. Conservation and applications of camphor tree (*Cinnamomum camphora*) in China: Ethnobotany and genetic resources. *Genet. Resour. Crop Evol.* **2016**, *63*, 1049–1061. [CrossRef]
6. Stubbs, B.J.; Specht, A.; Brushett, D. The essential oil of *Cinnamomum camphora* (L.) Nees and Eberm.—Variation in oil composition throughout the tree in two chemotypes from eastern Australia. *Int. J. Mol. Sci.* **2004**, *16*, 9–14.
7. Zhang, T.; Zheng, Y.; Fu, C.; Yang, H.; Liu, X.; Qiu, F.; Wang, X.; Wang, Z. Chemical variation and environmental influence on essential oil of *Cinnamomum camphora*. *Molecules* **2023**, *28*, 973. [CrossRef] [PubMed]

8. Guo, S.S.; Geng, Z.F.; Zhang, W.J.; Liang, J.Y.; Wang, C.F.; Deng, Z.W.; Du, S.S. The chemical composition of essential oils from *Cinnamomum camphora* and their insecticidal activity against the stored product pests. *Int. J. Mol. Sci.* **2016**, *17*, 1836. [CrossRef]
9. Jiang, H.; Wang, J.; Song, L.; Cao, X.S.; Yao, X.; Tang, F.; Yue, Y.D. GC×GC-TOFMS analysis of essential oils composition from leaves, twigs and seeds of *Cinnamomum camphora* L. Presl and their insecticidal and repellent activities. *Molecules* **2016**, *21*, 423. [CrossRef]
10. Sharifi-Rad, J.; Dey, A.; Koirala, N.; Shaheen, S.; El Omari, N.; Salehi, B.; Goloshvili, T.; Cirone Silva, N.; Bouyahya, A.; Vitalini, S. *Cinnamomum* species: Bridging phytochemistry knowledge, pharmacological properties and toxicological safety for health benefits. *Front. Pharmacol.* **2021**, *12*, 600139. [CrossRef] [PubMed]
11. Yang, J.; Lin, Q.; Fan, L.; Yang, N. High performance liquid chromatography–quadrupole time-of-flight mass spectrometry based metabolomic detection of non-volatile components of different chemotype of *Cinnamomum camphora*. *J. Anal. Chem.* **2020**, *75*, 1582–1588. [CrossRef]
12. Liu, Z.Z.; Kong, L.T.; Lu, S.B.; Zou, Z.R. Application of a combined homogenate and ultrasonic cavitation system for the efficient extraction of flavonoids from *Cinnamomum camphora* leaves and evaluation of their antioxidant activity in vitro. *J. Anal. Methods Chem.* **2019**, 4892635. [CrossRef]
13. Shen, N.; Wang, T.F.; Gan, Q.; Liu, S.; Wang, L.; Jin, B. Plant flavonoids: Classification, distribution, biosynthesis, and antioxidant activity. *Food Chem.* **2022**, *383*, 132531. [CrossRef]
14. Chen, S.; Wang, X.J.; Cheng, Y.; Gao, H.S.; Chen, X.H. A review of classification, biosynthesis, biological activities and potential applications of flavonoids. *Molecules* **2023**, *28*, 4982. [CrossRef] [PubMed]
15. Daryanavard, H.; Postiglione, A.E.; Mühlemann, J.K.; Muday, G.K. Flavonols modulate plant development, signaling, and stress responses. *Curr. Opin. Plant Biol.* **2023**, *72*, 102350. [CrossRef] [PubMed]
16. Billowria, K.; Ali, R.; Rangra, N.K.; Kumar, R.; Chawla, P.A. Bioactive flavonoids: A comprehensive review on pharmacokinetics and analytical aspects. *Crit. Rev. Anal. Chem.* **2024**, *54*, 1002–1016.
17. Jomova, K.; Alomar, S.Y.; Valko, R.; Liska, J.; Nepovimova, E.; Kuca, K.; Valko, M. Flavonoids and their role in oxidative stress, inflammation, and human diseases. *Chem. Biol. Interact.* **2025**, *413*, 111489.
18. Winkel-Shirley, B. Flavonoid Biosynthesis. A colorful model for genetics, biochemistry, cell biology, and biotechnology. *Plant Physiol.* **2001**, *126*, 485–493. [CrossRef]
19. Winkel, B.S.J. The Biosynthesis of Flavonoids. In *The Science of Flavonoids*; Springer: New York, NY, USA, 2006; pp. 71–96.
20. Quattrocchio, F.; Baudry, A.; Lepiniec, L.; Grotewold, E. The Regulation of Flavonoid Biosynthesis. In *The Science of Flavonoids*; Springer: New York, NY, USA, 2006; pp. 97–122.
21. Xue, J.; Lu, D.B.; Wang, S.G.; Lu, Z.H.; Liu, W.; Wang, X.F.; Fang, Z.Q.; He, X.Y. Integrated transcriptomic and metabolomic analysis provides insight into the regulation of leaf senescence in rice. *Sci. Rep.* **2021**, *11*, 14083. [CrossRef] [PubMed]
22. Chen, H.Y.; Yu, Y.; Sun, Q.W. Integrated transcriptomic and metabolomic analyses uncover regulatory networks and metabolite dynamics in *Cibotium barometz* leaf development. *Russ. J. Plant Physiol.* **2025**, *72*, 29. [CrossRef]
23. Tyagi, P.; Singh, D.; Mathur, S.; Singh, A.; Ranjan, R. Upcoming progress of transcriptomics studies on plants: An overview. *Front. Plant Sci.* **2022**, *13*, 1030890. [CrossRef]
24. Letertre, M.P.; Dervilly, G.; Giraudeau, P. Combined nuclear magnetic resonance spectroscopy and mass spectrometry approaches for metabolomics. *Anal. Chem.* **2020**, *93*, 500–518. [CrossRef]
25. Hua, Y.J.; Dai, B.Y.; Luo, Y.Y.; Ding, Y.J. Integrated analysis of multiple metabolome and transcriptome revealed the accumulation of flavonoids and associated molecular regulation mechanisms in *Rubus chingii* Hu at different developmental stages. *Plant Physiol Biochem.* **2023**, *204*, 108085.
26. Zheng, X.Y.; Zhu, Q.; Liu, Y.; Chen, J.X.; Wang, L.X.; Xiu, Y.; Zheng, H.Y.; Lin, S.Z.; Ling, P.; Tang, M.Q. Combined analysis of transcriptome and metabolome provides insights in response mechanism under heat stress in avocado (*Persea americana* Mill.). *Int. J. Mol. Sci.* **2024**, *25*, 10312. [CrossRef]
27. Wang, Q.C.; Shi, J.R.; Liu, J.N.; Zhang, P.; Li, L.; Xie, H.; Li, H.X.; Wang, H.X.; Liu, C.H.; Qin, P. Integration of transcriptome and metabolome reveals the accumulation of related metabolites and gene regulation networks during quinoa seed development. *Plant Mol. Biol.* **2024**, *114*, 10. [CrossRef] [PubMed]
28. Wei, C.; Liang, G.; Guo, Z.; Wang, W.; Zhang, H.; Liu, X.; Yu, S.; Xiong, L.; Luo, J. A novel integrated method for large-scale detection, identification, and quantification of widely targeted metabolites: Application in the study of rice metabolomics. *Mol. Plant* **2013**, *6*, 1769–1780. [CrossRef] [PubMed]
29. Alseekh, S.; Aharoni, A.; Brotman, Y.; Contrepois, K.; D'Auria, J.; Ewald, J.; Ewald, J.C.; Fraser, P.D.; Giavalisco, P.; Hall, R.D.; et al. Mass spectrometry-based metabolomics: A guide for annotation, quantification and best reporting practices. *Nat. Methods* **2021**, *18*, 747–756. [CrossRef] [PubMed]
30. Dao, D.; Fraser, A.N.; Hung, J.; Ljosa, V.; Singh, S.; Carpenter, A.E. CellProfiler Analyst: Interactive data exploration, analysis and classification of large biological image sets. *Bioinformatics* **2016**, *32*, 3210–3212. [CrossRef]

31. Chong, J.; Xia, J.G. MetaboAnalystR: An R package for flexible and reproducible analysis of metabolomics data. *Bioinformatics* **2018**, *34*, 4313–4314.
32. Kumar, R.; Ichihashi, Y.; Kimura, S.; Chitwood, D.H.; Headland, L.R.; Peng, J.; Maloof, J.N.; Sinha, N.R. A high-throughput method for Illumina RNA-Seq library preparation. *Front. Plant Sci.* **2012**, *3*, 202. [CrossRef]
33. Chen, S.F.; Zhou, Y.Q.; Chen, Y.; Gu, J. fastp: An ultra-fast all-in-one FASTQ preprocessor. *Bioinformatics* **2018**, *34*, i884–i890. [CrossRef]
34. Kim, D.; Langmead, B.; Salzberg, S.L. HISAT: A fast spliced aligner with low memory requirements. *Nat. Methods* **2015**, *12*, 357–360. [CrossRef] [PubMed]
35. Buchfink, B.; Xie, C.; Huson, D.H. Fast and sensitive protein alignment using DIAMOND. *Nat. Methods* **2015**, *12*, 59–60. [CrossRef]
36. Liao, Y.; Smyth, G.K.; Shi, W. featureCounts: An efficient general purpose program for assigning sequence reads to genomic features. *Bioinformatics* **2014**, *30*, 923–930. [CrossRef]
37. Love, M.I.; Huber, W.; Anders, S. Moderated estimation of fold change and dispersion for RNA-seq data with DESeq2. *Genome Biol.* **2014**, *15*, 550. [CrossRef]
38. Varet, H.; Brillet-Guéguen, L.; Coppée, J.Y.; Dillies, M.A. SARTools: A DESeq2-and EdgeR-based R pipeline for comprehensive differential analysis of RNA-Seq data. *PLoS ONE* **2016**, *11*, e0157022. [CrossRef] [PubMed]
39. Jin, J.; Zhang, H.; Kong, L.; Gao, G.; Luo, J. PlantTFDB 3.0: A portal for the functional and evolutionary study of plant transcription factors. *Nucleic Acids Res.* **2014**, *42*, D1182–D1187. [CrossRef] [PubMed]
40. Zheng, Y.; Jiao, C.; Sun, H.; Rosli, H.G.; Pombo, M.A.; Zhang, P.; Banf, M.; Dai, X.; Martin, G.B.; Giovannoni, J.J. iTAK: A program for genome-wide prediction and classification of plant transcription factors, transcriptional regulators, and protein kinases. *Mol. Plant* **2016**, *9*, 1667–1670. [CrossRef]
41. Dudoit, S.; Gentleman, R.C.; Quackenbush, J. Open source software for the analysis of microarray data. *BioTechniques* **2003**, *34*, S45–S51. [CrossRef]
42. Langfelder, P.; Horvath, S. WGCNA: An R package for weighted correlation network analysis. *BMC Bioinform.* **2008**, *9*, 559. [CrossRef]
43. Polanin, J.R.; Hennessy, E.A.; Tanner-Smith, E.E. A review of meta-analysis packages in R. *J. Educ. Behav. Stat.* **2017**, *42*, 206–242. [CrossRef]
44. Cline, M.S.; Smoot, M.; Cerami, E.; Kuchinsky, A.; Landys, N.; Workman, C.; Christmas, R.; Avila-Campilo, I.; Creech, M.; Gross, B. Integration of biological networks and gene expression data using Cytoscape. *Nat. Protoc.* **2007**, *2*, 2366–2382. [CrossRef]
45. Livak, K.J.; Schmittgen, T.D. Analysis of relative gene expression data using real-time quantitative PCR and the $2^{-\Delta\Delta CT}$ method. *Methods* **2001**, *25*, 402–408. [CrossRef] [PubMed]
46. Wang, L.; Wang, Q.G.; Fu, N.N.; Song, M.Y.; Han, X.; Yang, Q.; Zhang, Y.T.; Tong, Z.K.; Zhang, J.H. Cyanidin-3-O-glucoside contributes to leaf color change by regulating two bHLH transcription factors in *Phoebe bournei*. *Int. J. Mol. Sci.* **2023**, *24*, 3829. [CrossRef]
47. Yang, Y.; Chen, M.J.; Zhang, W.; Zhu, H.Y.; Li, H.; Niu, X.J.; Zhou, Z.S.; Hou, X.Y.; Zhu, J.L. Metabolome combined with transcriptome profiling reveals the dynamic changes in flavonoids in red and green leaves of *Populus*×*euramericana* 'Zhonghuahongye'. *Front. Plant Sci.* **2023**, *14*, 1274700. [CrossRef]
48. Song, S.S.; Tao, Y.; Gao, L.H.; Liang, H.L.; Tang, D.S.; Lin, J.; Wang, Y.C.; Gmitter Jr, F.G.; Li, C.F. An integrated metabolome and transcriptome analysis reveal the regulation mechanisms of flavonoid biosynthesis in a purple tea plant cultivar. *Front. Plant Sci.* **2022**, *13*, 880227. [CrossRef]
49. Zhong, Y.D.; Chen, C.H.; Gong, X.; Luan, X.Y.; Wu, Z.X.; Li, H.H.; Liu, Q.L.; Xu, M.; Yu, F.X. Transcriptome and metabolome analyses reveal a key role of the anthocyanin biosynthetic pathway cascade in the pigmentation of a *Cinnamomum camphora* red bark mutant ('Gantong 1'). *Ind. Crops Prod.* **2022**, *175*, 114236. [CrossRef]
50. Zhang, D.W.; Tan, Y.J.; Dong, F.; Zhang, Y.; Huang, Y.L.; Zhou, Y.Z.; Zhao, Z.J.; Yin, Q.; Xie, X.H.; Gao, X.W.; et al. The expression of IbMYB1 is essential to maintain the purple color of leaf and storage root in sweet potato [*Ipomoea batatas* (L.) Lam]. *Front. Plant Sci.* **2021**, *12*, 688707. [CrossRef] [PubMed]
51. Wu, X.X.; Li, Y.; Du, T.; Kang, L.; Pei, B.L.; Zhuang, W.B.; Tang, F. Transcriptome sequencing and anthocyanin metabolite analysis involved in leaf red color formation of *Cinnamomum camphora*. *Sci. Rep.* **2024**, *14*, 31470. [CrossRef]
52. Xie, N.; Guo, Q.Q.; Liao, M.Y.; Xiao, Y.; Fu, C.; An, Y.X. Transcriptome-wide identification of MYB gene family and functional analysis of *LcsMYB123* in *Litsea coreana var. sinensis*. *Plant Cell Tissue Organ Cult.* **2025**, *160*, 53. [CrossRef]
53. Han, H.; Zhang, L.; Zhao, R.; Li, S.; Wang, F.; Zhang, N.; Wang, X. Transcription factor CbbHLH147 improves alkali stress tolerance of *Cinnamomun bodinieri* by regulating flavonoid metabolism. *Gene* **2025**, *964*, 149629. [CrossRef] [PubMed]
54. Hichri, I.; Barrieu, F.; Bogs, J.; Kappel, C.; Delrot, S.; Lauvergeat, V. Recent advances in the transcriptional regulation of the flavonoid biosynthetic pathway. *J. Exp. Bot.* **2011**, *62*, 2465–2483. [CrossRef]
55. Zhao, L.; Gao, L.P.; Wang, H.X.; Chen, X.T.; Wang, Y.S.; Yang, H.; Wei, C.L.; Wan, X.C.; Xia, T. The R2R3-MYB, bHLH, WD40, and related transcription factors in flavonoid biosynthesis. *Funct. Integr. Genom.* **2013**, *13*, 75–98. [CrossRef]

56. Zhuo, M.G.; Wang, T.Y.; Huang, X.M.; Hu, G.B.; Zhou, B.Y.; Wang, H.C.; Abbas, F. ERF transcription factors govern anthocyanin biosynthesis in litchi pericarp by modulating the expression of anthocyanin biosynthesis genes. *Sci. Hortic.* **2024**, *337*, 113464. [CrossRef]
57. Wan, H.; Liu, Y.; Wang, T.; Jiang, P.; Wen, W.; Nie, J. Combined transcriptomic and metabolomic analyses identifies CsERF003, a citrus ERF transcription factor, as flavonoid activator. *Plant Sci.* **2023**, *334*, 111762. [CrossRef]
58. Hai, X.; Liu, G.; Lu, M.; Fan, R.; Li, K.; Guo, B.; Zhang, H.; Shang, F.; Han, Y. The AP2/ERF transcription factor OfERF2 promotes flavonoid biosynthesis in Osmanthus fragrans. *Tree Genet. Genomes* **2025**, *21*, 19. [CrossRef]
59. Gao, H.; Shi, M.; Zhang, H.; Shang, H.; Yang, Q. Integrated metabolomic and transcriptomic analyses revealed metabolite variations and regulatory networks in *Cinnamomum cassia* Presl from four growth years. *Front. Plant Sci.* **2024**, *14*, 1325961. [CrossRef]
60. Yang, Y.; Chen, M.G.; Liu, Y.X.; Ding, H.H.; Du, H.Y.; Sun, Z.Q.; Zhu, J.L. Metabolome and transcriptome analyses reveal different flavonoid biosynthesis and chlorophyll metabolism profiles between red leaf and green leaf of *Eucommia ulmoides*. *Forests* **2021**, *12*, 1260. [CrossRef]
61. Song, Y.T.; Zhang, G.Y.; Chen, N.; Zhang, J.G.; He, C.Y. Metabolomic and transcriptomic analyses provide insights into the flavonoid biosynthesis in sea buckthorn (*Hippophae rhamnoides* L.). *Lwt* **2023**, *187*, 115276. [CrossRef]
62. Murata, K.; Kitano, T.; Yoshimoto, R.; Takata, R.; Ube, N.; Ueno, K.; Ueno, M.; Yabuta, Y.; Teraishi, M.; Holland, C.K.; et al. Natural variation in the expression and catalytic activity of a naringenin 7-O-methyltransferase influences antifungal defenses in diverse rice cultivars. *Plant J.* **2020**, *101*, 1103–1117. [CrossRef] [PubMed]
63. Xu, H.P.; Zhang, S.Y.; Liang, C.L.; Li, M.; Wang, R.; Song, J.K.; Cui, Z.H.; Yang, Y.J.; Liu, J.L.; Li, D.L. Melatonin enhances resistance to *Botryosphaeria dothidea* in pear by promoting jasmonic acid and phlorizin biosynthesis. *BMC Plant Biol.* **2024**, *24*, 470. [CrossRef]
64. Duan, C.B.; Hou, J.Y.; Zhao, X.Y.; Xu, H.L.; Jiang, E.Y.; Wang, N.N.; Chen, Z.X.; Gao, J.; Bian, Q.; Chen, L.Z.; et al. Why is it so clean under the apple trees: Discovery of novel phloretin derivatives as potential herbicidal agents. *Pest Manag. Sci.* **2025**, *81*, 3762–3773. [CrossRef]
65. Ji, Z.K.; Deng, W.; Chen, D.; Liu, Z.D.; Shen, Y.C.; Dai, J.M.; Zhou, H.; Zhang, M.; Xu, H.C.; Dai, B. Recent understanding of the mechanisms of the biological activities of hesperidin and hesperetin and their therapeutic effects on diseases. *Heliyon* **2024**, *10*, e26862. [CrossRef] [PubMed]
66. Damasceno, R.O.S.; Pinheiro, J.L.S.; Silva, L.D.D.; Rodrigues, L.H.M.; Emídio, J.J.; Lima, T.C.; Sousa, D.P.D. Phytochemistry and anti-inflammatory and antioxidant activities of *Cinnamomum osmophloeum* and its bioactive constituents: A review. *Plants* **2025**, *14*, 562. [CrossRef] [PubMed]
67. Kamle, M.; Mahato, D.K.; Lee, K.E.; Bajpai, V.K.; Gajurel, P.R.; Gu, K.S.; Kumar, P. Ethnopharmacological properties and medicinal uses of *Litsea cubeba*. *Plants* **2019**, *8*, 150. [CrossRef] [PubMed]
68. Ekom, S.E.; Tamokou, J.D.D.; Kuete, V. Methanol extract from the seeds of *Persea americana* displays antibacterial and wound healing activities in rat model. *J. Ethnopharmacol.* **2022**, *282*, 114573. [CrossRef]

Disclaimer/Publisher's Note: The statements, opinions and data contained in all publications are solely those of the individual author(s) and contributor(s) and not of MDPI and/or the editor(s). MDPI and/or the editor(s) disclaim responsibility for any injury to people or property resulting from any ideas, methods, instructions or products referred to in the content.